# THE EUROPEAN PHYSICAL JOURNAL A



Regular Article - Theoretical Physics

### From the slow to the rapid neutron capture process

Friedrich-Karl Thielemann<sup>1,2,a</sup>

<sup>1</sup> Department of Physics, University of Basel, Klingelbergstrasse 82, 4056 Basel, Switzerland

Received: 13 October 2022 / Accepted: 9 January 2023 / Published online: 30 January 2023

© The Author(s) 2023

Communicated by Nicolas Alamanos

**Abstract** This contribution starts with memories about Franz Käppeler, as a human being and a scientist, his impact on neutron capture nucleosynthesis via experiments and astrophysical studies, before extending from his focus (the s-process) to the r-process, discussing its mechanism, related astrophysical sites and examining in a concluding section its role during galactic evolution.

#### 1 Introduction

Before starting the science related to this article, let me say a few words about Franz. He has been a highlight in terms of science, excellence, creative thinking, diligence, and character. We met first at one of the Ringberg Workshops in Nuclear Astrophysics, where he participated together with his colleagues Hermann Beer and Klaus Wisshack. One of the important decisions regarding his science was that he turned from measurements of nuclear cross sections for reactor applications to neutron captures in astrophysics. The idea (in 1988) to utilize the <sup>7</sup>Li(p,n)-reaction to provide a neutron spectrum which corresponds to a Maxwellian neutron energy distribution, equivalent to a thermal environment of kT = 25.3keV [1], was revolutionary and permitted to measure directly already energy/velocity-averaged neutron capture rates for typical s-process conditions. This and his enormous productivity, filling a number of Atomic and Nuclear Data volumes [2-4], which were then readily applied to s-process studies [5–7], led to a tremendous impact in that fields, spreading from Karlsruhe around the world, including finally also nToF at CERN [8,9]. Franz was a centerpiece of the field, he brought the second Nuclei in the Cosmos (II) conference to Karlruhe, educated a large family of students who are now at important places world-wide, and collaborated energetically with many colleagues, covering experiments as well as theory. I am proud of 14 joint publications, a nice Nuclear and Particle Science review with him and Michael Wiescher [10], and we had a joint graduate student [Iris Dillmann, [11,12]]. Shortly after I returned from the US to Europe in 1994, I took the freeway from Frankfurt/Darmstadt to Basel (my then new home) and decided to pick an exit to visit Franz' home, which I had known from previous visits. It was a surprise for all of us, finding a joyful group of visitors, Michael Wiescher and Roberto Gallino were visiting for joint work [13]. Figure 1 (right panel) is testimony of this highly enjoyable encounter.

## 2 What features determine the outcome of neutron capture processes?

Franz has mostly worked on the s-process, i.e. slow neutron captures, where - if the resulting isotope is unstable - the beta-decay wins in the majority of cases, and one can just think of a sequence of neutron captures connecting nuclei A and A+1. The identification of a participating isotope is then unique for each A, as one can essentially think of the beta-decay of an instantaneous transition in comparison to neutron captures. Therefore, the speed of the build-up of heavy elements is determined by neutron capture cross sections / rates with the slowest reactions for small cross sections related to the smallest reaction Q-values at magic neutron numbers.

If neutron densities  $n_n$  are enhanced, the rates increase proportional to the neutron density and neutron capture life times (proportional to  $1/n_n$ ) can become shorter than the beta-decay of unstable nuclei. We display this behavior in Fig. 2 for an abundance composition starting with initial solar abundance for  $^{127}$ I,  $^{235}$ U and  $^{238}$ U in an environment with a neutron density of  $n_n = 6 \times 10^{18}$  cm<sup>-3</sup>. One can see that within less than  $10^{-4}$ s neutron captures hit the limiting isotopes of the nuclear network utilized here.

This leads to the two major neutron capture processes, the s-and the r-process which are both indicated in Fig. 3. (A modification of the s-process at slightly higher neutron den-



<sup>&</sup>lt;sup>2</sup> GSI Helmholtz Center for Heavy Ion Research, Planckstrasse 1, 64291 Darmstadt, Germany

<sup>&</sup>lt;sup>a</sup> e-mail: f-k.thielemann@unibas.ch (corresponding author)

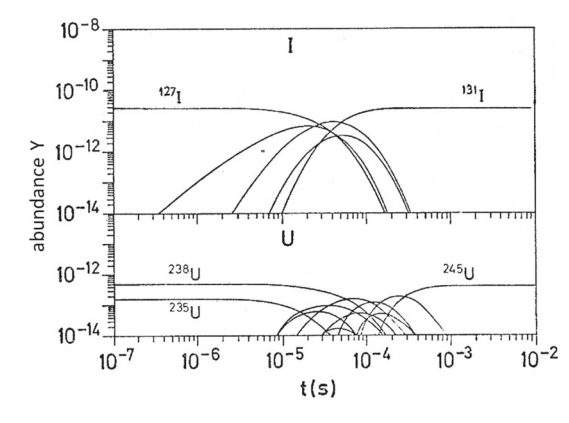
12 Page 2 of 14 Eur. Phys. J. A (2023) 59:12





Fig. 1 Left: Franz Käppeler, Klaus Wisshak, Hermann Beer, Marcel Arnould, Claus Rolfs at NIC-0 in Crete (organized by Claus Rolfs in 1988), which motivated Heinz Oberhummer to start the NIC series with NIC-I 2 years later. Right: Franz and Rosel Käppeler with Roberto Gallino and Michael Wiescher at the dinner table in Franz' beautiful

home, overlooking the Rhine valley from the Kraichgau heights [working on [13]]. BTW, Franz had smuggled Rosel in a Fiat 500, hidden below the back seat, from East to West Germany long before the fall of the Berlin wall. He was not only creative, but had an enormous courage



**Fig. 2** Starting from solar abundances of  $^{127}$ I,  $^{235}$ U and  $^{238}$ U, in a plasma with a neutronen density of  $n_n = 6 \times 10^{18}$  cm<sup>-3</sup> and a temperature of  $10^9$ K, it takes typically less than  $10^{-4}$ s until neutron captures hit the limiting isotopes included in the nucleosynthesis network

sities with  $n_n$  up to  $10^{16} \text{cm}^{-3}$ , the i-process, is discussed in the chapter by Falk Herwig. In that case the unique identification of a mass number A with a specific isotope is lost, as branchings with comparable beta-decay lifetimes come into place). The rapid neutron capture process is not only dominated by fast neutron captures, in most conditions the inverse photo-disintegrations play an essential role as well. For a reaction  $i(n, \gamma)m$ , with i standing for nucleus (Z, A) and m for (Z, A + 1), the relation between the forward rate  $\langle \sigma v \rangle_{i;n,\gamma}$  and the photodisintegration rate  $\lambda_{m;\gamma,n}$  is given by

$$\lambda_{m;\gamma,n}(T) = \frac{g_n G_i}{G_m} \left(\frac{\mu_{in} kT}{2\pi \hbar^2}\right)^{3/2} \exp(-Q_{i;n,\gamma}/kT) \langle \sigma v \rangle_{i;n,\gamma}, \tag{1}$$

containing the reduced mass  $\mu_{in}$  and the neutron capture Q-value for the reaction,  $g_n = 2 \times (1/2) + 1$  for the neutrons and the partition functions G for the nuclei involved. In chemical equilibrium the difference between forward neutron capture

and backward photodisintegration flux for nucleus i vanishes, i.e.  $\dot{Y}_i = -n_n \langle \sigma v \rangle_{i;n,\gamma} Y_i + \lambda_{m;\gamma,n} Y_m = 0$ . Making also use of the relation between  $\langle \sigma v \rangle_{i;n,\gamma}$  and  $\lambda_{m;\gamma,n}$ , based on detailed balance, results in

$$\frac{Y_m}{Y_i} = n_n \frac{G_m}{2G_i} \left\lceil \frac{A_m}{A_i} \right\rceil^{3/2} \left\lceil \frac{2\pi\hbar^2}{m_u k T} \right\rceil^{3/2} \exp\left(\frac{Q_{i;n,\gamma}}{k T}\right). \tag{2}$$

For the two adjacent isotopes (Z, A) and (Z, A+1) or (Z, N) and (Z, N+1), connected by neutron capture, the Q-value is equivalent to the neutron separation energy  $S_n$  of (Z, A+1). Equation(2) leads to an abundance distribution in an isotopic chain for element Z with a maximum at a unique neutron separation energy, identical for all different elements Z. This leads to a process path along a contour line for a specific neutron separation energy  $S_n$  which depends on the neutron density  $n_n$  and the temperature T. A specific choice with a typical  $S_n \approx 2 \text{MeV}$  is shown in Fig. 3, which indicates the main difference between s- and r-process features.

The s-process (with neutron number densities  $n_n$  of  $10^6$ to 10<sup>11</sup> cm<sup>-3</sup>) is strongly affected by neutron captures with the smallest rates, leading to the slowest process speed and abundance pile-ups at neutron magic numbers for nuclei at or close to stability. In the r-process (with neutron densities  $n_n > 10^{20} \,\mathrm{cm}^{-3}$ ) the neutron captures are extremely fast (see Fig. 2) which is also the case for reverse photodisintegrations of very neutron-rich nuclei with temperatures in excess of  $10^9$ K. Therefore, a chemical or  $(n, \gamma) - (\gamma, n)$  equilibrium is obtained (almost) instantaneously for each isotopic chain Z. The process speed is determined by the beta-decay rates between isotopic chains for nuclei at the position of the rprocess path, i.e. those at contour lines of constant neutron separation energies. These contour lines experience kinks at closed neutron shells (far from stability) with longest halflives for the points closest to stability, i.e. at the top of these



Eur. Phys. J. A (2023) 59:12 Page 3 of 14 12

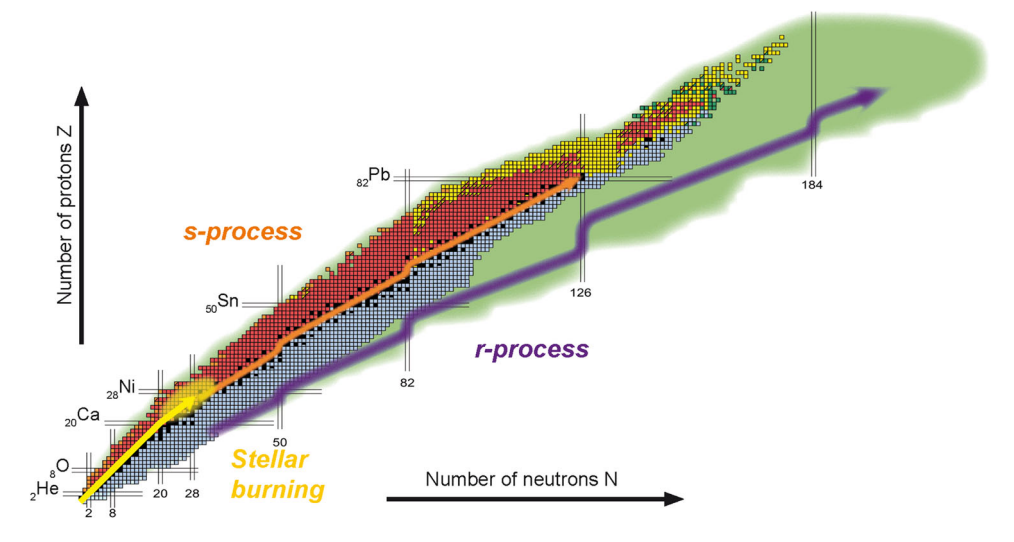


**Fig. 3** (courtesy EMMI, GSI/Different Arts) Nuclear chart with major nucleosynthesis processes, (i) the formation of elements up to Fe, Ni, Zn in fusion reactions during stellar evolution and explosions, (ii) the s-process path along stability up to Pb and Bi, and (iii) the (later to be discussed) r-process path. Stable nuclei are indicated by black squares, experimentally known  $\beta^+$ -unstable nuclei by red squares,  $\beta^-$ -unstable

nuclei by blue squares, alpha-unstable nuclei by yellow squares. The area of  $\beta$ -unstable nuclei which are still stable against neutron or proton emission, as predicted by nuclear mass models, appear in a light green shade. Horizontal or vertical lines stand for neutron or proton shell closures, N=8, 20, 28, 50, 82, 126, 184 and Z=8, 20, 26, 28, 50, 82 (, 114), the one in brackets not shown here

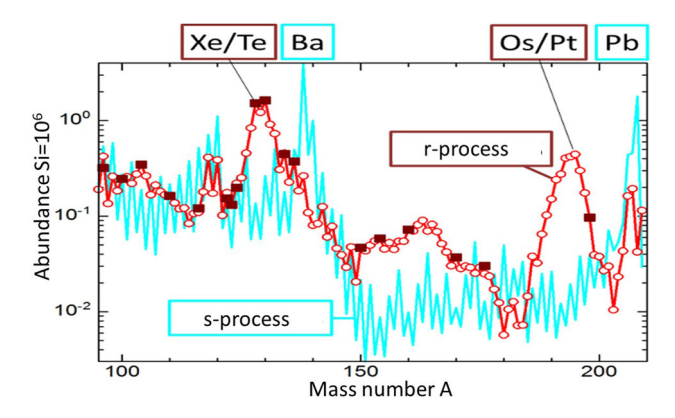


**Fig. 4** adapted from [14]: solar s-process abundances (blue), resulting from a superposition of stellar s-process sources [6]. The subtraction from global solar abundances provides the abundance contributions due to the remaining processes which create heavy nuclei up to the actinides, mainly the before-mentioned and later discussed r-process (red)

kinks. Therefore, the abundance maxima of the r-process are shifted to the left of the s-process maxima, because the beta-decay of isotopes at the top of these kinks leads to isotopes at stability with a smaller A. This is shown in Fig. 4.

We know from the ample amount of Franz Käppeler's work, that the solar s-process contribution is caused by a superposition of several processes, i.e. the weak and strong s-process from massive and low to intermediate mass stars (with variations according to the contributions from the stellar mass interval as well as the stellar metallicity which determines the neutron to Fe-seed ratio of this secondary nucleosynthesis process). Opposite to this it has long been believed

that the solar r-process abundances are due to unique process features. The following sections will discuss this in more detail, combined with an attempt to present an overview of the present understanding of the possible astrophysical sites, with the result that also the solar r-process abundances are caused by a superposition of different contributions.

#### 3 The r-process in explosive burning

#### 3.1 Initial complete chemical equilibrium, NSE

Opposite to the s-process, which works on typical neutroncapture timescales of months to years with neutrons being produced via  $(\alpha, n)$ -reactions during stellar evolution, the high density of neutrons (with a half-life of the order 10 min), required for an r-process to occur, indicate an explosive environment. This starts typically with a subset of explosive Si-burning, where temperatures in excess of  $5-6\times10^9$ K are attained, leading initially to a nuclear statistical equilibrium, i.e. a complete set of chemical equilibria, balancing all forward and backward flows in reactions, in particular also for proton or neutron capture reactions  $p + (Z, A) \rightleftharpoons (Z + 1, A + 1) + \gamma$  and  $n + (Z, A) \rightleftharpoons$  $(Z, A + 1) + \gamma$ , corresponding to a relation between the chemical potentials  $\mu_p + \mu(Z, A) = \mu(Z + 1, A + 1)$  and  $\mu_n + \mu(Z, A) = \mu(Z, A + 1)$ , because the chemical potential of photons vanishes. Such relations between the chemical potentials lead to identical equations for abundance ratios as



12 Page 4 of 14 Eur. Phys. J. A (2023) 59:12

given for neutron captures in Eq.(2), derived there via expressions for the reaction rates. If this is not only the case for a particular reaction, but across the whole nuclear chart, the complete reaction sequence is in chemical equilibrium, i.e.  $Z\mu_p + N\mu_n = \mu(Z,A)$ , termed complete chemical or also nuclear statistical equilibrium NSE [e.g. [15,16]]. For Boltzmann distributions (which apply in general in astrophysical plasmas, with the exception of highly degenerate conditions, where Fermi distributions have to be utilized for the chemical potentials), the abundances of nuclei can be expressed by nuclear properties like the binding energies  $B_i(Z_i, A_i)$ , the abundances of free neutrons and protons  $Y_n$  and  $Y_p$ , and environment conditions like temperatures T and densities  $\rho$ , leading to the abundance of nucleus i [with  $Z_i$  protons and  $N_i$  neutrons or  $A_i = Z_i + N_i$  nucleons, see e.g.[15]]

$$Y_{i} = Y_{n}^{N_{i}} Y_{p}^{Z_{i}} \frac{G_{i}(T) A_{i}^{3/2}}{2^{A_{i}}} \left(\frac{\rho}{m_{u}}\right)^{A_{i}-1} \times \left(\frac{2\pi\hbar^{2}}{m_{u}kT}\right)^{3(A_{i}-1)/2} \exp\left(\frac{B_{i}}{kT}\right), \tag{3}$$

where  $G_i$  corresponds to the partition function of nucleus i, as the ground and excited state population is in thermal equilibrium. Reactions moderated by the weak interaction, i.e.  $\beta$ -decays, electron captures, and charged-current neutrino interactions, change the overall proton to nucleon ratio  $Y_e = \sum Z_i Y_i / \sum A_i Y_i = \sum Z_i Y_i$  (also called electron fraction) and occur on longer time scales than particle captures and photodisintegrations. They are not necessarily in equilibrium and have to be followed explicitly. Thus, as a function of time the NSE will follow the corresponding densities  $\rho(t)$ , temperatures T(t), and  $Y_e(t)$ , determining the two unknowns  $Y_n$  and  $Y_p$  as a solution of the equations for total mass conservation and  $Y_e$  resulting from weak interactions

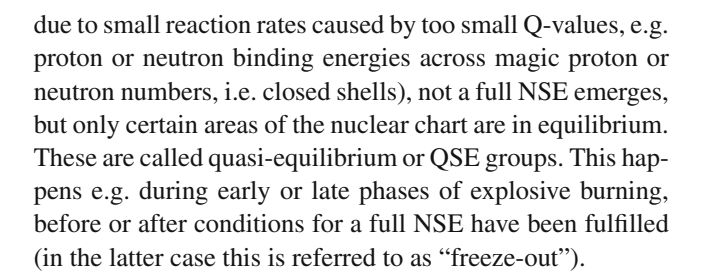
$$\sum_{i} A_{i} Y_{i} = Y_{n} + Y_{p}$$

$$+ \sum_{i,(A_{i}>1)} (Z_{i} + N_{i}) Y_{i}(\rho, T, Y_{n}, Y_{p}) = 1$$

$$\sum_{i} Z_{i} Y_{i} = Y_{p} + \sum_{i,(Z_{i}>1)} Z_{i} Y_{i}(\rho, T, Y_{n}, Y_{p}) = Y_{e}.$$
(4)

This permits then the prediction of the individual nuclear abundances  $Y_i$  from Eq.(3). In general, very high densities favor large nuclei, due to the high power of  $\rho^{A_i-1}$ , and very high temperatures favor light nuclei, due to  $(kT)^{-3(A_i-1)/2}$  in Eq. (3). In the intermediate regime  $\exp(B_i/kT)$  favors tightly bound nuclei with the highest binding energies in the mass range A=50–60 of the Fe-group, but depending on the given  $Y_e$ . The width of the composition distribution is determined by the temperature.

Under certain conditions, i.e. not sufficiently high temperatures, when not all reactions are fast enough (especially



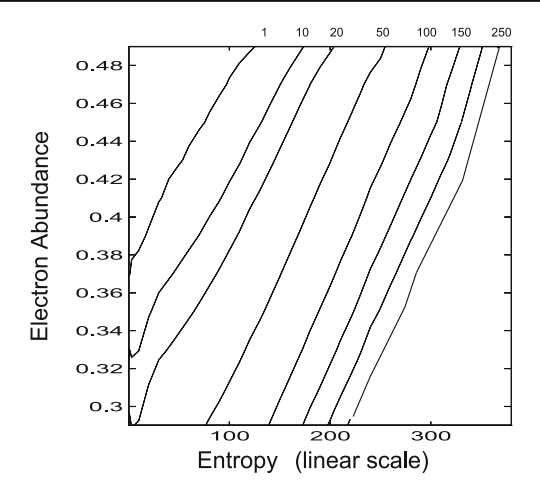
### 3.2 Charged-particle freeze-out from NSE and the resulting n/seed ratio

In general, r-process environment pass initially through a full NSE, but depending on the initial entropy (combining density  $\rho$  and temperature T), a so-called normal freeze-out (ending with the NSE composition for the freeze-out temperature) or an alpha-rich freeze-out takes place, when during the decline from high temperatures not all alpha-particles can be incorporated into heavy nuclei on the small timescale before the freeze-out of reactions takes place [see Fig. 11 in [17]]. The requirement for an r-process to proceed afterwards covers neutron/seed ratios of 10 to 150 after freeze-out of charged particle reactions in order to produce all (from the light to the heaviest) r-process nuclei via neutron capture from seed abundances. This translates for a normal freeze-out into  $Y_e = 0.12 - 0.3$ . Alternatively, for a moderate  $Y_e > 0.40$ an extremely alpha-rich freeze-out is needed [see for details the discussion in [17]]. Under the latter conditions the large mass fraction in  ${}^{4}$ He (with N=Z) would permit ratios of remaining free neutrons to (small) abundances of heavier seed nuclei, which are sufficiently high to attain r-process conditions. This is shown in detail in Fig. 5.

After charged-particle (normal or alpha-rich) freeze-out, OSE-groups of neutron captures and photodisintegrations are formed along the isotopic chains of heavy elements during the working of the r-process, as discussed in the previous section in Eq.(2). This is an approximate behavior, in reality full network calculations with all necessary nuclear input are needed. But such an approximation gives clues to a full understanding of the results. Exemptions from this behavior can occur in the late r-process phases, when also neutron capture reactions and photodisintegrations start to freeze-out from equilibrium and final neutron captures can reshape the abundance curves. The main conclusion from this discussion is that the characteristics of an r-process are determined by the combination of entropy S and  $Y_e$  (and an expansion timescale for a close to adiabatic expansion from the initial densities and temperatures determining S). For moderate  $Y_e$ 's only very high entropies can support an r-process which proceeds up to the actinides, while a low  $Y_e$  - like in neutron star matter - supports a full r-process already for the lowest entropies. The r-process results for various astrophysical



Eur. Phys. J. A (2023) 59:12 Page 5 of 14 12



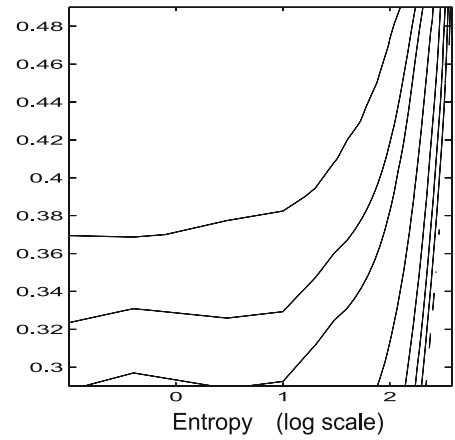


Fig. 5 neutron-to-seed ratios (shown as contour lines) resulting in expanding hot plasmas from explosive burning as a function of the electron abundance  $Y_e$  and the entropy (measured in  $k_b$  per baryon). A strong r-process, producing the actinides with n/seed of 150, requires for moderate  $Y_e$ 's of about 0.45, entropies beyond 250 [18]. The alter-

native is that for vanishing entropies (right panel), i.e. cold matter like in neutron stars, the n/seed curves turn over and become independent of entropy. Then an n/seed ratio of 150 requires a  $Y_e$  of about 0.15 or less. Image reproduced with permission from [18], copyright by AAS

environments, spanning a possible continuum between these extremes, reflect directly these connections.

#### 3.3 What determines $Y_e$ ?

This leaves us with the causes for the initial values of entropy and  $Y_e$ . While in some cases the initial  $Y_e$  is set by the starting abundance composition like in neutron star ejecta (where their small  $Y_e$  was obtained previously at high densities by capture of electrons with high Fermi energies on protons and nuclei), in many environments neutrinos play a significant role which dial the initial  $Y_e$  before the expansion from maximum temperatures and densities. This is due to neutrino and antineutrino capture on neutrons and protons  $v_e + n \rightarrow p + e^-$ ,  $\bar{v}_e + p \rightarrow n + e^+$ , where for similar neutrino and antineutrino energies the first reaction wins and leads to an increase of  $Y_e$ . The equilibrium electron fraction for environments with neutrino-driven outflows reads [19,20]

$$Y_e^{\text{eq}} \approx \left[ 1 + \frac{L_{\bar{\nu}_e} \left( \epsilon_{\bar{\nu}_e} - 2\Delta + 1.2\Delta^2 / \epsilon_{\bar{\nu}_e} \right)}{L_{\nu_e} \left( \epsilon_{\nu_e} + 2\Delta + 1.2\Delta^2 / \epsilon_{\nu_e} \right)} \right]^{-1}$$

$$\approx \left[ 1 + \left( \frac{\epsilon_{\bar{\nu}_e}}{\epsilon_{\nu_e}} \right) \left( \frac{L_{\bar{\nu}_e}}{L_{\nu_e}} \right) \right]^{-1}.$$
(5)

Here,  $\Delta=1.293$  MeV is the neutron-proton mass difference,  $\epsilon=\langle E^2\rangle/\langle E\rangle$  relates to neutrino energies, and L to their luminosities. In the approximation on the right we have assumed that neutrino energies are large enough so that, to acceptable accuracy, the terms containing  $\Delta$  can be neglected. The above given general considerations are the ones which then directly enter into r-process nucleosynthesis for specific environments.

#### 3.4 Nuclear properties

In addition to the astrophysical environments, determining these starting conditions, the nuclear physics aspects (nuclear mass models far from stability,  $\beta$ -decay half-lives and delayed neutron emission, fission, neutron captures and photodisintegrations determining the final abundances during neutron freeze-out, direct capture contributions,  $\alpha$ -decays of the final abundances) enter decisively in producing the abundance pattern of the r-process. Major aspects are related to experimental progress in accessing unstable nuclei far from stability, combined with a growing theoretical understanding of their properties. Without giving here a substantial number of related references, these issues are discussed in extended detail in a recent Reviews of Modern Physics article [17] and from experimental as well as theoretical points of view in the chapters by Ani Aprahamian and by Gabriel Martinez-Pinedo and Karlheinz Langanke in the present volume.



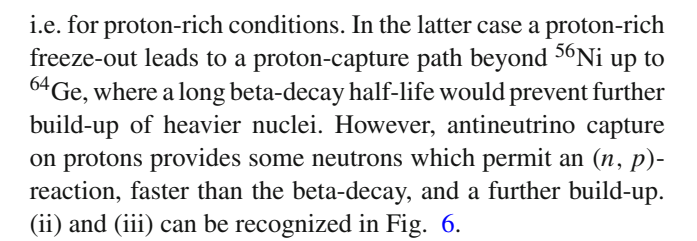
12 Page 6 of 14 Eur. Phys. J. A (2023) 59:12

#### 4 Suggested astrophysical sites

#### 4.1 Neutrino-driven core-collapse supernovae

The present volume does not contain a specific chapter on core-collapse supernovae and their explosion mechanism, driven by energy deposition going back to neutrinos streaming out of the collapsed proto-neutron star. We refer here to recent review articles [21,22]. The explodability and an overview on final results of the core collapse of massive stars, ending in regular core-collapse supernovae and neutron stars or in black holes has been given e.g. in [23]. The neutrino and antineutrino capture on neutrons and protons is the key ingredient for energy deposition and the supernova explosion mechanism. Thus, combined with the impact on  $Y_e$ , neutrinos - as discussed in the previous section - play a central role in determining the conditions of the innermost ejecta of core-collapse supernovae for their nucleosynthesis (i.e. the three parameters electron fraction  $Y_e$ , entropy S, and expansion time scale  $\tau$ ) from the dynamics of the explosion. Mass accreted through the (standing) shock during the early phase of the explosion gets dissociated into nucleons and alpha particles, depending on the temperature of the shock. This material can flow down to the proto-neutron star or stay in the neutrino heated region and expands. In spherically symmetric simulations, the accretion takes place only in the first second after bounce while in multidimensional simulations downflows stay active during several seconds, providing a continuous nucleosynthesis source. In general, the matter ejected comes from two regions: the surface of the proto-neutron star and the layers which have experiences the outgoing shock. The outer layers of the proto-neutron star and the matter that has been accreted on its surface can be ejected by neutrinos. When this ejection occurs after accretion flows are terminated and the outflow becomes supersonic, this is known as a neutrino-driven wind, suggested initially as the r-process site [see e.g. [19,24] for reviews and references]. Thus, the neutrinos do not only deposit the necessary energy to unbind and eject material, they can also change  $Y_e$  and change neutrons into protons when neutrino capture wins over antineutrino capture, preventing this way an r-process to occur.

The nucleosynthesis follows the pathway described in the previous section: early on an NSE is attained until the charged-particle freeze-out leads to a seed distribution and the neutron-to-seed  $(Y_n/Y_{\rm seed})$  or possibly a proton-to-seed  $(Y_p/Y_{\rm seed})$  ratio, depending on  $Y_e$  being smaller or larger than 0.5. At temperatures around  $3 \times 10^9$  K three processes are possible: (i) a (strong) r-process [18,20,26,27] if  $Y_n/Y_{\rm seed} > 100$  [which does not generally occur in neutrino-driven supernovae, opposite to what was expected initially [28,29]], (ii) a weak r-process [24,25,30,31], if  $Y_n/Y_{\rm seed} \sim 1$ , or (iii) a  $v_p$ -process [e.g. [25,32]], if  $Y_n/Y_{\rm seed}$  is very small and  $Y_p > Y_n$ ,



#### 4.2 Magneto-rotationally driven supernovae

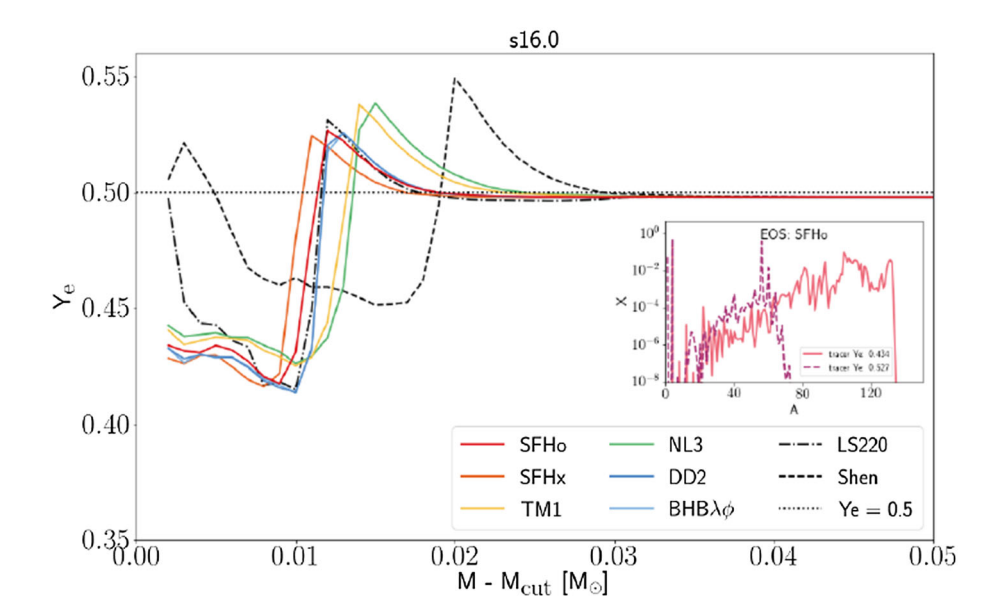
In addition to neutrino-driven explosions, observations of very energetic supernovae [33], long gamma-ray bursts (GRB) [34], pulsars with extremely high magnetic fields [magnetars [35,36]] indicate the key role of magnetic fields in some explosions, here summarized under the name of so-called magneto-rotational supernovae (MR-SN). There are very energetic explosion known as hypernovae (HN) [37] with nucleosynthesis features different from regular core-collapse supernovae [38] that reach energies of about  $\sim 10^{52}$  erg which cannot be explained by the neutrino-driven mechanism. These HNe are associated to the collapse of massive stars with  $> 30 - 40 M_{\odot}$ , which probably lead to blackhole formation. In all these cases magnetic fields and rotation play a dominant role in the explosion mechanism, which can end either with a central highly magnetized neutron star (magnetar) or alternatively a central stellar-mass black hole. In this subsection we will concentrate on the first subclass of magneto-rotational supernovae, while in the following subsection we will focus on the second case with black hole formation (collapsars or also GRB supernovae), often in the literature identified with hypernovae.

The magneto-rotational mechanism, proposed in the 1970 s, relies on the impact of rotation and magnetic fields on the core-collapse and explosion phase. MR-SNe were proposed by [39] and later by [40] as an r-process site. First simulations, although ignoring or simplifying the neutrino treatment, found a successful r-process in 2D [41] and 3D [42]. Rapid rotation of the iron core is necessary, which leads to an amplification of the magnetic field by rotational winding, being possibly aided by magneto-rotational instabilites (MRI) [43]. After bounce, the strong magnetic pressure launches jets along the rotational axis [e.g. [31,42,44,45]]. However, some 3D models lead to kink instabilities and the formation of less collimated bipolar jets [46,47]. This is the case if the initial pre-collapse magnetic fields are not sufficiently high and the winding of magnetic fields during the collapse does not support an immediate ejection of neutronrich matter along the rotation axis. In this case neutrino interactions enhance  $Y_e$  before the MRI-effects lead to enhanced magnetic field strengths up to a value which permits ejection and explosion. Based on this, the initial results by [42], starting with pre-collapse magnetic fields of 10<sup>12</sup>G and leading to a full strong r-process up to the actinides, might have been



Eur. Phys. J. A (2023) 59:12 Page 7 of 14 12

Fig. 6 Innermost ejecta composition from a  $16\,M_{\odot}$ core-collapse supernova explosion, resulting in moderately low  $Y_e$ -matter from collapse and moderately proton-rich conditions due to neutrino interactions during the explosion [shown for simulations with different equations of state [25]]. This leads to a weak r-process and a vp-process with abundance distributions shown in the insert. Image reproduced with permission from [25], copyright by the authors



too optimistic for typical conditions as presented in [31] or [48].

A fully self-consistent treatment of these processes requires high resolution simulations which can resolve magnetorotational instabilities (MRI) and predict reliably the possible amplification of magnetic fields during the explosion. Present calculations depend on the quality of high-resolution 3D magneohydrodynamics plus the uncertain and therefore assumed initial conditions [49], that either cause strong jet ejection or can develop kink instabilities of the jets. Based on initial conditions, somewhat parametrized in terms of the impact, either neutrino heating or magnetic pressure is causing the supernova explosion. This is related to the question whether very high magnetic fields exist from the beginning of the collapse or are only later developing due the the MRI instability. The latter delays the polar ejection of matter, exposing it longer to neutrinos from the collapse and reducing the neutron-richness of matter and the strength of the r-process. Thus, the production for heavy neutron capture elements varies strongly, being either Fe and Zn dominated like in regular core-collapse SNe or Eu dominated, indicating a strong r-process. This is shown in Fig. 7.

Our present conclusions would be that magneto-rotational supernovae which lead to neutron stars will on average only cause a relatively weak r-process, but further investigations are needed [49].

#### 4.3 Collapsars leading to GRB supernovae/hypernovae

Other potential r-process sites associated with a magnetorotational core collapse are due to the accretion discs that form surrounding a massive black hole, originating from the collapse of a massive star with high rotation (a collapsar). Pioneering nucleosynthesis studies [50] have demonstrated

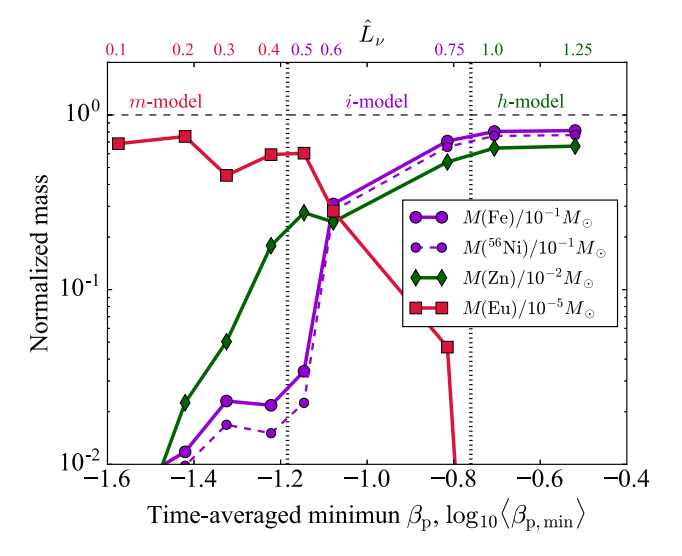


**Fig. 7** Nucleosynthesic features of rotating core-collapse SN models (h, i-, i, i+, m) with varying ratios of neutrino luminosity and magnetic field strengths. Model m represents a strong MHD-jet supernova. One can see the transition from a regular core-collapse SN pattern, dominated by  $^{56}$ Ni, total Fe (after decay), and Zn, to a strong r-process pattern with a high Eu abundance. Image reproduced with permission from [31], copyright by AAS

that also here neutrinos can play a critical role. While the possibilities for an r-process in recent studies are not conclusive, yet, we discuss here this option in further detail.

Opposite to the above early studies, an interesting question is related to whether some environments can actually cause an actinide boost, i.e. a very strong r-process with large actinide abundance, while others produce a normal solar-type r-process distribution. Recent studies [51] conclude that actinides are substantially overproduced relative to lanthanides for  $Y_e$ -values in the range 0.1–0.15, sensitive



12 Page 8 of 14 Eur. Phys. J. A (2023) 59:12

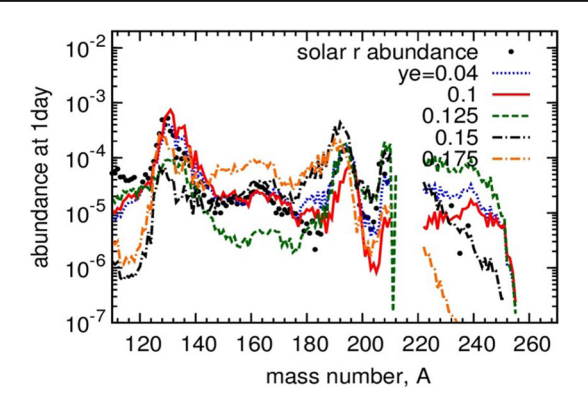


**Fig. 8** Abundances predictions by Wu as a function of the mass number A at  $10^9$  s after an r-process event for different initial  $Y_e$ 's, focusing on low  $Y_e$  values and their influence on the abundances of actinides. Image reproduced with permission from [53], copyright by the authors

to the influence of fission cycling. This is consistent with other studies [52,53, see Fig. 8], which find, for a variety of nuclear mass models, that electron fractions in the range of  $\sim 0.15$  are most favorable to explain "actinide boost" matter. Given that "actinide boost" compositions depend on a dominant fraction of the ejecta to originate from a very narrow  $Y_e$ -range in order to reproduce their observed abundance pattern, requires that nature produces a restricted range of conditions where such  $Y_e$ -values occur. While to date this question is not settled, we want to discuss here a possibility, recently suggested in [54], based on the equilibrium electron fractions  $Y_e$  presented already in Eq.(5).

If a black hole is present or forms, the neutrino irradiation is dramatically quenched and the gas flow around the BH regulates itself into a state of mild electron degeneracy. Due to negative feedback between electron degeneracy and neutrino cooling (higher degeneracy leads to fewer electrons and positrons, therefore reducing the neutrino emission, this leads to a higher temperature and thus to a lowering of the degeneracy), the disk midplane settles inside of the inner  $\sim 10 \, GM_{\rm BH}/c^2$  to electron fractions of  $Y_e \approx 0.1$  [55]. Interestingly, this occurs once the accretion rates exceed an "ignition value" that depends on the BH spin [56] and the corresponding accretion rates are those that are needed to power (long or short) GRBs [57]. While discovered in semianalytic models, this self-regularization to low  $Y_e$ -values in the disk midplane is also found in full-fledged numerical (magneto-)hydrodynamic simulations [see e.g. [58–60]].

The simulation of such neutrino-cooled accretion flows is a major challenge since one needs to resolve the small length scales of the magneto-rotational instability [61] and to evolve the black hole torus system for a very large number of dynamical time scales (up to several seconds, while the dynamical time scales are  $\sim$  ms). Therefore, it is not entirely surprising that the exploration of this topic is still in initial stages, that large parts of the relevant parameter space are not explored

yet and, where parameters are comparable, the results do not yet agree (at least not concerning the ejecta composition). The currently existing GRMHD explorations [58,59,62,63] agree that a large fraction ( $\sim 40\%$ ) of the initial torus mass becomes unbound, but to date there is no agreement about the resulting  $Y_e$  and composition of the ejecta. For example, [59] find  $Y_e$  values around 0.12, those of [58] peak around  $\sim 0.14$ , while [63] find a broad distribution between 0.2 and 0.4. Despite a still missing consensus about the ejecta properties, we think that the black hole torus idea for the source of "actinide boost" material is compelling.

The progenitor systems of actinide boost material could then come from massive accretion disks around black holes, forming substantial tori (either from low mass black holes or large BH spins) and, potentially, also collapsar accretion disks. If black hole torus systems indeed manage to eject matter with properties similar to what they produce robustly in their inner torus regions, and a black hole is needed to launch an (either long or short) GRB (rather than, say, a magnetized neutron star), then it would be the GRB engines that produce the "actinide boost" matter [64].

#### 4.4 Neutron star and neutron star black hole mergers

A number of proposals for producing the heaviest (r-process) nuclei in Nature have come forward over the years. These include especially neutron star mergers, going back to early suggestions [65–67], and concrete predictions for resulting abundance features [see e.g. [68], for a review before the observation of GW170817]. The follow-up of the gravitational wave event GW170817 [69] revealed strong electromagnetic emission in the aftermath of the merger and showed in particular the expected signatures of an r-process powered kilonova. The decay of its bolometric lightcurve agreed well with the expectations for radioactive heating rates from a broad range of r-process elements [70–73]. Observations of the 2017 kilonova showed that it was initially blue, indicating the synthesis of elements lighter than barium (Z = 56)[74,75]. These elements have low densities of atomic levels and make the medium less opaque, allowing light to escape (decouple from matter) earlier and without having lost too much energy. The presence of lighter r-process elements was also confirmed by the direct observation of strontium (Z =38) in the spectra [76]. After a few days, the light turned from blue to red, pointing to the presence of lanthanides and actinides [further reviews are given in [17,73,77–80]].

Based on these considerations, three components of neutron star merger ejecta contribute to the overall nucleosynthesis site: (i) dynamical ejecta including compressed and shock heated material from the initial collision as well as possible – cold – tidal spiral arm-type ejecta, (ii) winds driven by neutrinos (emitted from the central hot very massive neutron star - until black hole formation - and the accretion disk) and



Eur. Phys. J. A (2023) 59:12 Page 9 of 14 12

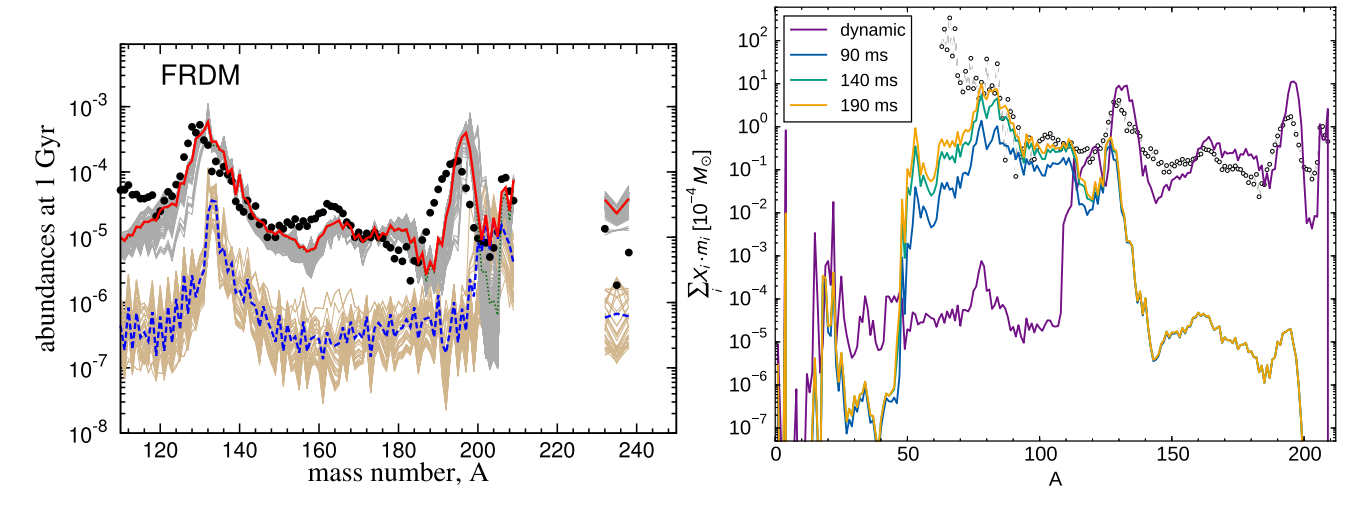
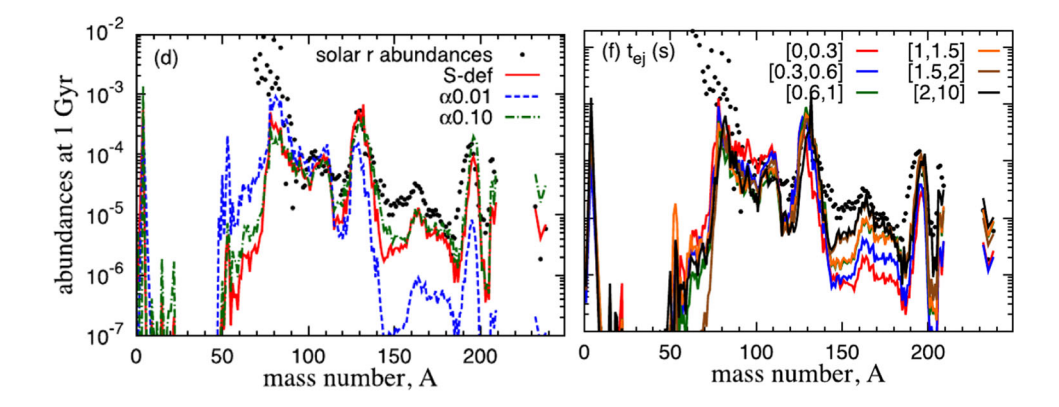


Fig. 9 Abundance comparison between BNS merger models and solar r-process abundances: (left) for dynamical ejecta (i) based on [81], (right) a combination of tidally dominated dynamical ejecta [82] and abundance yields from neutrino-driven wind ejecta (ii) for different massive NS lifetimes until black hole formation after the merger [83]. In the left panel dark gray and brown lines correspond to cold r-process

conditions from slow tidal ejecta and to hot r-process conditions from shock-heated fast ejecta. Averaged lines for all trajectories are marked in red, for the fast ejecta in blue. Image reproduced with permission from [81], copyright by APS (left) and from [83], copyright by AAS (right)

Fig. 10 Abundance comparison between BNS merger models and solar system r-process. Left panel: viscous disk ejecta with various viscosity paramters  $\alpha$ , showing the intensity of r-processing. Right panel: top model of the left panel (which overall reproduces solar r-abundances) with integrated ejecta compositions as a function of integration time since merging. Image reproduced with permission from [84], copyright by Oxford University Press



potentially also by magnetic fields, and (iii) finally mass outflow from the black hole accretion disk. A common feature of these scenarios is that matter reaches NSE with  $Y_e$  given by weak reactions or in the cold dynamical ejecta component by beta equilibrium in the cold neutron stars before the merger.

Combining the three types of ejecta (and their nucleosynthesis features) discussed above with kilonova lightcurve and spectra observations, there is no doubt that neutron star mergers are indeed a major r-process source. The blue emission points to the production of a light (lanthanide-free) r-process in dynamical and wind ejecta of Fig. 9, affected by neutrino interactions enhancing the related  $Y_e$  of (i) and (ii), while the late red emission is the natural outcome for heavy (lanthanides and beyond) r-process ejecta from accretion disk outflows with low  $Y_e$  (iii, see Fig. 10). The r-process outcome as a function of  $Y_e$  is discussed in detail in refs. [83–91]. In summary, there is strong evidence that this neutron star merger event has produced at least a broad, and maybe

the whole, r-process range. However, based on the observed lanthanide fraction  $X_{\text{La}}$ , [92] find that at least for the neutron star merger GW170817 this does not represent a typical solar r-process pattern.

### 5 Galactic chemical evolution of neutron capture elements

We have gone in this article through a number of astrophysical sites responsible for neutron capture elements, especially concentrating on the r-process. There exist many observations of individual objects, which hint at their ejecta compositions, from supernovae and their remnants, from neutron star mergers, and from indirect investigations via meteoritic inclusions, just to name a few. However, there exists also an integrated view, how all these additions changed the composition of the interstellar gas out of which the next genera-



12 Page 10 of 14 Eur. Phys. J. A (2023) 59:12

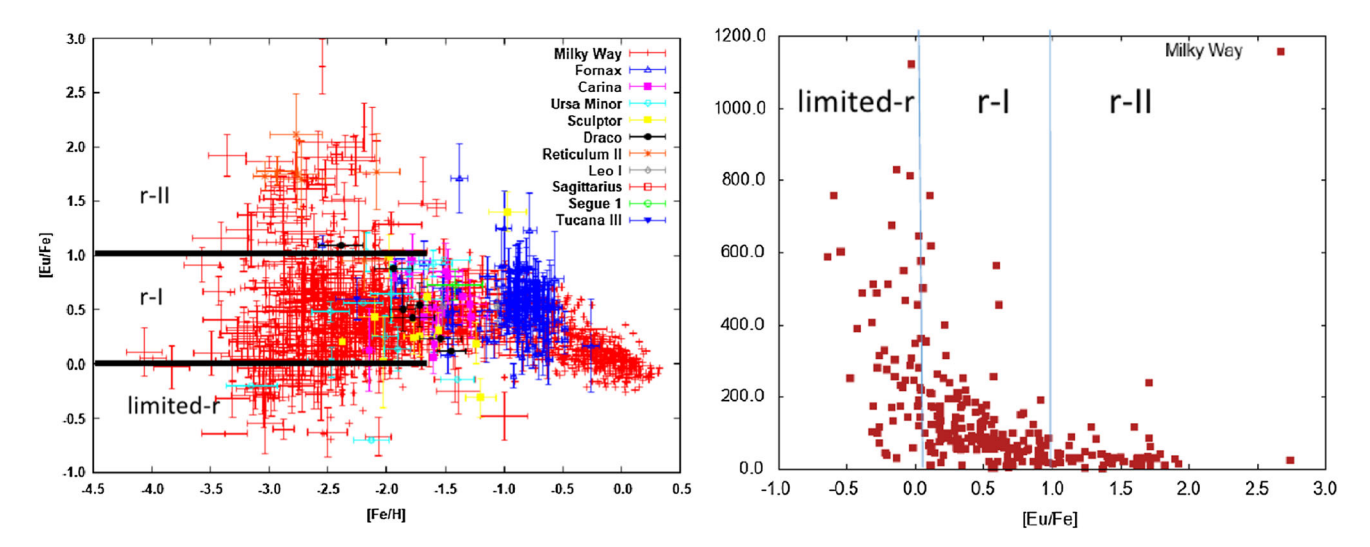


**Fig. 11** Left: [Eu/Fe] ratios of 1572 stars with Eu detections from the SAGA database [103]. A huge scatter can be observed before at about [Fe/H] = -2 an averaging (smaller spread) sets in, which continues with a different gradient when SNe Ia start to contribute at -1. Right: Sr/Eu ratios for all stars with [Fe/H] < -2.5, which show a drastic change

at about [Eu/Fe] = 0-0.3, i.e. the division between limited-r stars and r-enriched r-I and r-II stars [for these observational classifications, and also the definition of actinide boost stars, see e.g. [104–113]]. Image adapted from [54], copyright by the authors

tions of stars formed. This evolution of element abundances in galaxies (chemical evolution) has been pioneered in the 1960s to 1980s and described in a number of books, e.g. [93,94], discussing this evolution as a function of [Fe/H] which measures logarithmically the Fe/H ratio in comparison to solar ratios, i.e. with a value of 0 for a solar composition and e.g. -2 for 1/100 of solar. Core-collapse supernovae, originating from massive stars, have a short delay time until explosion and enter early in galactic evolution. The first features can already be seen down to extreme cases at [Fe/H] = - 6. They produce lots of O, Ne, Mg in the outer zones during stellar evolution and Si, S, Ar, Ca, as well as Ti and <sup>56,57,58</sup>Ni (<sup>56,57</sup>Ni decaying to Fe) in the explosively processed zones during the passing of the explosion shock wave. Their ratio of these "alpha-elements" (O, Ne, Mg, Si, S, Ar, Ca, Ti) to Fe is about a factor of 3 higher than in the solar composition. Type Ia supernovae (not discussed here), originating from intermediate mass stars and experiencing a delay due to binary evolution, show an impact with their strong Fe contributions only at about [Fe/H] = -1. These two aspects are the dominant features in galactic evolution, its understanding evolved over the years [for recent general overviews see [95–100]].

The production of the heavier elements, i.e. the s-process and specifically the r-process, has been the focus of this contribution. The role of the weak or main s-process in massive or low and intermediate mass stars has been discussed by other authors in this volume. The overall relation of the s-process vs. r-process impact can be viewed as a function of metallicity. The dominant s-process contribution comes from low and intermediate mass stars with long evolution-

ary lifetimes, therefore entering late in galactic evolution. A figure of observed La/Eu ratios as a function of metallicity in [101] underlines the general tendency that the abundance ratio is at low metallicities dominated by the r-process contribution, while the combination with the delayed s-process leads finally to solar ratios. This supports the understanding that at the lowest metallicities (for [Fe/H]<-2.5) abundance features represent solar r-process ratios, before during the later evolution also s-contributions enter, leading eventually to the solar abundance ratios.

The possible sites of r-process nucleosynthesis have been presented in the previous section, including neutron star mergers, magneto-rotational jet supernovae and collapsars. Quark-deconfinement (QD) supernovae [102] have recently also been suggested as another weak r-process site. We will now have a look at their impact in galactic evolution, examining especially Eu (a typical r-process element, strongly dominated by the r-process contribution) and Sr (pointing to weak r-process contributions).

Figure 11 shows, dependent on the [Eu/Fe]-ratio categorized into limited-r and r-enriched r-I and r-II stars, that the observations of low-metallicity stars proof the existence of a weak or limited r-process, while most stars show r-process enhanced abundance patterns. This goes together with a variation of e.g. the Sr/Eu ratio, ranging from about 1120 down to 0.5 [110], indicating the different decline of the abundance curve as a function of *A*. Some of the r-process enriched stars show an "actinide boost", i.e. their Th or U to Eu ratio is supersolar [found in most cases for r-II stars, [51,106,107,109,114]].



Eur. Phys. J. A (2023) 59:12 Page 11 of 14 12

In summary: We have discussed a number of suggested rprocess sites, but only one of them is proven by a direct observation of the explosive event. Observations of low metallicity stars show essentially three types of patterns, a weak or limited r-process, a strong solar-type r-process, and an actinide-boosted r-process [for reviews and impact on galactic chemical evolution see e.g. [17,54,80,115–119]]. There exist strong indications that the weak r-process pattern is related to core-collapse supernovae (probably mostly due to magneto-rotational version?). Whether the latter two types are produced in different sites or result from variations within the same site (e.g. neutron star mergers) is still debated. The question is now how to identify features which can point back to individual sites. In terms of chemical evolution models it is important to utilize methods that can treat the impact of rare events and test whether the sizable spread in abundance ratios in Fig. 11 is due to different origins or just the result of an inhomogeneous environment, going back to rare events in the early galaxy.

A promising approach is to look for correlations among different elements, especially in relation to Fe [54,120]. Recent data from the SAGA and JINA databases [103, 121], presented in Fig. 11, permit a correlation between Eu and Fe for [Eu/Fe]<0-0.3, i.e. for stars with lower than average r-process enrichment which also show high [Sr/Fe] values. Interpreted in a straight-forward way this would point to a negligible Fe/Eu ratio (in comparison to solar ratios) in the major r-process sources (like e.g. neutron star mergers and collapsars), while a noticeable co-production of Fe with Eu is possible in less strong r-process sources, e.g. with a weak r-process (probably pointing to rare supernova types). The latter options have been discussed in more detail in [54], possibly linking limited-r stars to (rare) supernovae, r-I stars mainly to neutron star mergers, and r-II stars to collapsars. Alternative views, trying to relate the entire r-process abundances to neutron star mergers alone have been presented recently [114,122–124]. Such a type of interpretation requires further and continuous consistency checks through observations, modelling of the contributing objects, and the treatment of their impact in galactic evolution.

**Acknowledgements** This publication benefitted highly from collaborations and exchange within the European Cost Action CA16117 "Chemical Evolution as Tracers of the Evolution of the Cosmos" (ChETEC) and the "International Research Network for Nuclear Astrophysics" (IReNA).

Funding Information Open access funding provided by University of Basel

**Data availability statement** This manuscript has no associated data or the data will not be deposited. [Authors' comment: This manuscript has the style of a review and does not provide data predictions or observational results. For predictions see the cited literature, for observations the SAGA and JINA databases [103,121].]

Open Access This article is licensed under a Creative Commons Attribution 4.0 International License, which permits use, sharing, adaptation, distribution and reproduction in any medium or format, as long as you give appropriate credit to the original author(s) and the source, provide a link to the Creative Commons licence, and indicate if changes were made. The images or other third party material in this article are included in the article's Creative Commons licence, unless indicated otherwise in a credit line to the material. If material is not included in the article's Creative Commons licence and your intended use is not permitted by statutory regulation or exceeds the permitted use, you will need to obtain permission directly from the copyright holder. To view a copy of this licence, visit http://creativecommons.org/licenses/by/4.0/.

#### References

- W. Ratynski, F. Käppeler, Phys. Rev. C 37(2), 595 (1988). https://doi.org/10.1103/PhysRevC.37.595
- Z.Y. Bao, F. Käppeler, At. Data Nucl. Data Tables 36, 411 (1987). https://doi.org/10.1016/0092-640X(87)90011-8
- Z.Y. Bao, H. Beer, F. Käppeler, F. Voss, K. Wisshak, Nucl. Phys. A 621, 595 (1997). https://doi.org/10.1016/ S0375-9474(97)00310-2
- Z.Y. Bao, H. Beer, F. Käppeler, F. Voss, K. Wisshak, T. Rauscher, At. Nucl. Data Tables 76(1), 70 (2000). https://doi.org/10.1006/adnd.2000.0838
- F. Kappeler, H. Beer, K. Wisshak, Rep. Prog. Phys. 52(8), 945 (1989). https://doi.org/10.1088/0034-4885/52/8/002
- C. Arlandini, F. Käppeler, K. Wisshak, R. Gallino, M. Lugaro, M. Busso, O. Straniero, Astrophys. J. 525(2), 886 (1999). https://doi.org/10.1086/307938
- F. Käppeler, R. Gallino, S. Bisterzo, W. Aoki, Rev. Mod. Phys. 83(1), 157 (2011). https://doi.org/10.1103/RevModPhys.83.157
- R. Reifarth, C. Lederer, F. Käppeler, J. Phys. G 41, 053101 (2014). https://doi.org/10.1088/0954-3899/41/5/053101
- N. Colonna, F. Gunsing, F. Käppeler, Prog. Part. Nucl. Phys. 101, 177 (2018). https://doi.org/10.1016/j.ppnp.2018.02.002
- F. Käppeler, F.K. Thielemann, M. Wiescher, Ann. Rev. Nucl. Part. Sci. 48, 175 (1998). https://doi.org/10.1146/annurev.nucl. 48.1.175
- I. Dillmann et al., Capture Gamma-Ray Spectroscopy and Related Topics. Am. Inst. Phys. Conf. Ser. 819, 123–127 (2006). https://doi.org/10.1063/1.2187846
- I. Dillmann, T. Rauscher, M. Heil, F. Käppeler, W. Rapp, F.K. Thielemann, J. Phys. G 35(1), 014029 (2008). https://doi.org/10. 1088/0954-3899/35/1/014029
- F. Käppeler, M. Wiescher, U. Giesen, J. Goerres, I. Baraffe, M. El Eid, C.M. Raiteri, M. Busso, R. Gallino, M. Limongi, A. Chieffi, Astrophys. J. 437, 396 (1994). https://doi.org/10.1086/175004
- J.J. Cowan, F.K. Thielemann, Phys. Today 57(10), 10–47 (2004). https://doi.org/10.1063/1.1825268
- D.D. Clayton, Principles of Stellar Evolution and Nucleosynthesis (McGraw-Hill, New York, 1968) (Reissued by University of Chicago Press, Chicago, 1983)
- 16. W.R. Hix, F.K. Thielemann, Astrophys. J. 511, 862 (1999)
- J.J. Cowan, C. Sneden, J.E. Lawler, A. Aprahamian, M. Wiescher, K. Langanke, G. Martínez-Pinedo, F.K. Thielemann, Rev. Mod. Phys. 93(1), 015002 (2021). https://doi.org/10.1103/RevModPhys.93.015002
- C. Freiburghaus, J.F. Rembges, T. Rauscher, E. Kolbe, F.K. Thielemann, K.L. Kratz, B. Pfeiffer, J.J. Cowan, Astrophys. J. 516, 381 (1999). https://doi.org/10.1086/307072
- Y.Z. Qian, S.E. Woosley, Astrophys. J. 471, 331 (1996). https://doi.org/10.1086/177973



12 Page 12 of 14 Eur. Phys. J. A (2023) 59:12

 R.D. Hoffman, S.E. Woosley, Y.Z. Qian, Astrophys. J. 482(2), 951 (1997). https://doi.org/10.1086/304181

- B. Müller, Annu. Rev. Nucl. Part. Sci. 69, 253 (2019). https://doi. org/10.1146/annurev-nucl-101918-023434
- A. Burrows, D. Vartanyan, Nature 589(7840), 29 (2021). https://doi.org/10.1038/s41586-020-03059-w
- K. Ebinger, S. Curtis, S. Ghosh, C. Fröhlich, M. Hempel, A. Perego, M. Liebendörfer, F.K. Thielemann, Astrophys. J. 888(2), 91 (2020). https://doi.org/10.3847/1538-4357/ab5dcb
- A. Arcones, F.K. Thielemann, J. Phys. G 40(1), 013201 (2013). https://doi.org/10.1088/0954-3899/40/1/013201
- S. Ghosh, N. Wolfe, C. Fröhlich, Astrophys. J. 929(1), 43 (2022). https://doi.org/10.3847/1538-4357/ac4d20
- T.A. Thompson, A. Burrows, B.S. Meyer, Astrophys. J. 562, 887 (2001). https://doi.org/10.1086/323861
- K. Farouqi, K. Kratz, B. Pfeiffer, T. Rauscher, F. Thielemann, J.W. Truran, Astrophys. J. 712, 1359 (2010). https://doi.org/10.1088/ 0004-637X/712/2/1359
- S.E. Woosley, J.R. Wilson, G.J. Mathews, R.D. Hoffman, B.S. Meyer, Astrophys. J. 433, 229 (1994). https://doi.org/10.1086/ 174638
- K. Takahashi, J. Witti, H.T. Janka, Astron. Astrophys. 286, 857 (1994)
- A. Arcones, J. Bliss, J. Phys. G 41(4), 044005 (2014). https://doi. org/10.1088/0954-3899/41/4/044005
- N. Nishimura, H. Sawai, T. Takiwaki, S. Yamada, F.K. Thielemann, Astrophys. J. 836, L21 (2017). https://doi.org/10.3847/2041-8213/aa5dee
- C. Fröhlich, G. Martínez-Pinedo, M. Liebendörfer, F.K. Thielemann, E. Bravo, W.R. Hix, K. Langanke, N.T. Zinner, Phys. Rev. Lett. 96(14), 142502 (2006). https://doi.org/10.1103/PhysRevLett.96.142502
- K. Nomoto, M. Tanaka, N. Tominaga, K. Maeda, New Astron. Rev. 54(3–6), 191 (2010). https://doi.org/10.1016/j.newar.2010. 09.022
- S.E. Woosley, J.S. Bloom, Ann. Rev. Astron. Astrophys.
   44(1), 507 (2006). https://doi.org/10.1146/annurev.astro.43.
   072103.150558
- M. Kramer, Cosmic magnetic fields: from planets, to stars and galaxies, in *IAU Symposium*, vol. 259, ed. by K.G. Strassmeier, A.G. Kosovichev, J.E. Beckman (Springer, 2009), pp.485–492. https://doi.org/10.1017/S1743921309031159
- J. Greiner et al., Nature 523, 189 (2015). https://doi.org/10.1038/ nature14579
- K. Iwamoto et al., Nature 395, 672 (1998). https://doi.org/10. 1038/27155
- T. Nakamura, H. Umeda, K. Iwamoto, K. Nomoto, M.A. Hashimoto, W.R. Hix, F.K. Thielemann, Astrophys. J. 555, 880 (2001). https://doi.org/10.1086/321495
- J.M. LeBlanc, J.R. Wilson, Astrophys. J. 161, 541 (1970). https://doi.org/10.1086/150558
- A.G.W. Cameron, Astrophys. J. 587, 327 (2003). https://doi.org/ 10.1086/368110
- S. Nishimura, K. Kotake, M.A. Hashimoto, S. Yamada, N. Nishimura, S. Fujimoto, K. Sato, Astrophys. J. 642, 410 (2006). https://doi.org/10.1086/500786
- C. Winteler, R. Käppeli, A. Perego, A. Arcones, N. Vasset, N. Nishimura, M. Liebendörfer, F.K. Thielemann, Astrophys. J. Lett. 750, L22 (2012)
- M. Obergaulinger, P. Cerdá-Durán, E. Müller, M.A. Aloy, Astron. Astrophys. 498(1), 241 (2009). https://doi.org/10.1051/ 0004-6361/200811323
- P. Mösta, S. Richers, C.D. Ott, R. Haas, A.L. Piro, K. Boydstun,
   E. Abdikamalov, C. Reisswig, E. Schnetter, Astrophys. J. Lett.
   785, L29 (2014). https://doi.org/10.1088/2041-8205/785/2/L29

- M. Obergaulinger, H.T. Janka, M.A. Aloy, MNRAS 445, 3169 (2014). https://doi.org/10.1093/mnras/stu1969
- P. Mösta, L.F. Roberts, G. Halevi, C.D. Ott, J. Lippuner, R. Haas,
   E. Schnetter, Astrophys. J. 864, 171 (2018). https://doi.org/10.3847/1538-4357/aad6ec
- T. Kuroda, A. Arcones, T. Takiwaki, K. Kotake, Astrophys. J. 896(2), 102 (2020). https://doi.org/10.3847/1538-4357/ab9308
- M. Reichert, M. Obergaulinger, M. Eichler, M.Á. Aloy, A. Arcones, MNRAS 501(4), 5733 (2021). https://doi.org/10.1093/mnras/stab029
- M. Reichert, M. Obergaulinger, M.Á. Aloy, M. Gabler, A. Arcones, F.K. Thielemann, MNRAS 518(1), 1557 (2023). https://doi.org/10.1093/mnras/stac3185
- R. Surman, G.C. McLaughlin, W.R. Hix, Astrophys. J. 643(2), 1057 (2006). https://doi.org/10.1086/501116
- E.M. Holmbeck, T.M. Sprouse, M.R. Mumpower, N. Vassh, R. Surman, T.C. Beers, T. Kawano, Astrophys. J. 870, 23 (2019). https://doi.org/10.3847/1538-4357/aaefef
- M. Eichler, W. Sayar, A. Arcones, T. Rauscher, Astrophys. J. 879, 47 (2019). https://doi.org/10.3847/1538-4357/ab24cf
- F.K. Thielemann, B. Wehmeyer, M.R. Wu, J. Phys. Conf. Ser. 1668, 012044 (2020). https://doi.org/10.1088/1742-6596/1668/ 1/012044
- K. Farouqi, F.K. Thielemann, S. Rosswog, K.L. Kratz, Astron. Astrophys. 663, A70 (2022). https://doi.org/10.1051/0004-6361/ 202141038
- A.M. Beloborodov, Astrophys. J. 588, 931 (2003). https://doi.org/ 10.1086/374217
- W. Chen, A.M. Beloborodov, Astrophys. J. 657, 383 (2007). https://doi.org/10.1086/508923
- W.H. Lee, E. Ramirez-Ruiz, New J. Phys. 9, 17 (2007). https://doi.org/10.1088/1367-2630/9/1/017
- D.M. Siegel, B.D. Metzger, Astrophys. J. 858, 52 (2018). https://doi.org/10.3847/1538-4357/aabaec
- R. Fernández, A. Tchekhovskoy, E. Quataert, F. Foucart, D. Kasen, MNRAS 482, 3373 (2019). https://doi.org/10.1093/mnras/sty2932
- D.M. Siegel, A. Agarwal, J. Barnes, B.D. Metzger, M. Renzo, V.A. Villar, Astrophys. J. 941(1), 100 (2022). https://doi.org/10. 3847/1538-4357/ac8d04
- 61. S.A. Balbus, J.F. Hawley, Rev. Mod. Phys. 70, 1 (1998)
- D.M. Siegel, B.D. Metzger, Phys. Rev. Lett. 119, 231102 (2017). https://doi.org/10.1103/PhysRevLett.119.231102
- J.M. Miller, T.M. Sprouse, C.L. Fryer, B.R. Ryan, J.C. Dolence, M.R. Mumpower, R. Surman, Astrophys. J. 902(1), 66 (2020). https://doi.org/10.3847/1538-4357/abb4e3
- D.M. Siegel, Nat. Rev. Phys. (2022). https://doi.org/10.1038/ s42254-022-00439-1
- J.M. Lattimer, D.N. Schramm, Astrophys. J. 192, L145 (1974). https://doi.org/10.1086/181612
- J.M. Lattimer, D.N. Schramm, Astrophys. J. 210, 549 (1976). https://doi.org/10.1086/154860
- 67. D. Eichler, M. Livio, T. Piran, D.N. Schramm, Nature **340**, 126 (1989). https://doi.org/10.1038/340126a0
- F.K. Thielemann, M. Eichler, I.V. Panov, B. Wehmeyer, Ann. Rev. Nucl. Part. Sci. 67, 253 (2017). https://doi.org/10.1146/annurev-nucl-101916-123246
- B.P. Abbott et al., Phys. Rev. Lett. 119, 161101 (2017). https://doi.org/10.1103/PhysRevLett.119.161101
- B.D. Metzger, G. Martínez-Pinedo, S. Darbha, E. Quataert, A. Arcones, D. Kasen, R. Thomas, P. Nugent, I.V. Panov, N.T. Zinner, MNRAS 406, 2650 (2010). https://doi.org/10.1111/j.1365-2966. 2010.16864.x
- S. Rosswog, J. Sollerman, U. Feindt, A. Goobar, O. Korobkin, R. Wollaeger, C. Fremling, M.M. Kasliwal, Astron. Astrophys. 615, A132 (2018). https://doi.org/10.1051/0004-6361/201732117



Eur. Phys. J. A (2023) 59:12 Page 13 of 14 12

- Y. Zhu et al., Astrophys. J. 863, L23 (2018). https://doi.org/10. 3847/2041-8213/aad5de
- B.D. Metzger, Living Rev. Relativ. 23, 1 (2019). https://doi.org/ 10.1007/s41114-019-0024-0
- D. Kasen, B. Metzger, J. Barnes, E. Quataert, E. Ramirez-Ruiz, Nature 551, 80 (2017). https://doi.org/10.1038/nature24453
- P.A. Evans et al., Science 358, 1565 (2017). https://doi.org/10. 1126/science.aap9580
- D. Watson, C.J. Hansen, J. Selsing, A. Koch, D.B. Malesani, A.C. Andersen, J.P.U. Fynbo, A. Arcones, A. Bauswein, S. Covino, A. Grado, K.E. Heintz, L. Hunt, C. Kouveliotou, G. Leloudas, A.J. Levan, P. Mazzali, E. Pian, Nature 574, 497 (2019). https://doi.org/10.1038/s41586-019-1676-3
- M.M. Kasliwal, D. Kasen, R.M. Lau, D.A. Perley, S. Rosswog, E.O. Ofek, K. Hotokezaka, R.R. Chary, J. Sollerman, A. Goobar, D.L. Kaplan, Mon. Not. R. Astron. Soc. Lett. (2019). https://doi. org/10.1093/mnrasl/slz007
- 78. C.J. Horowitz et al., J. Phys. G **46**, 083001 (2019). https://doi.org/ 10.1088/1361-6471/ab0849
- M. Shibata, K. Hotokezaka, Ann. Rev. Nucl. Part. Sci. 69, 41 (2019). https://doi.org/10.1146/annurev-nucl-101918-023625
- 80. A. Perego, F.K. Thielemann, G. Cescutti, Handb. Gravit. Wave Astron. (2021). https://doi.org/10.1007/978-981-15-4702-7\_13-1
- J.J. Mendoza-Temis, M.R. Wu, K. Langanke, G. Martínez-Pinedo, A. Bauswein, H.T. Janka, Phys. Rev. C 92, 055805 (2015). https://doi.org/10.1103/PhysRevC.92.055805
- O. Korobkin, S. Rosswog, A. Arcones, C. Winteler, MNRAS 426, 1940 (2012). https://doi.org/10.1111/j.1365-2966.2012.21859.x
- D. Martin, A. Perego, A. Arcones, F.K. Thielemann, O. Korobkin, S. Rosswog, Astrophys. J. 813, 2 (2015). https://doi.org/10.1088/ 0004-637X/813/1/2
- M.R. Wu, R. Fernández, G. Martínez-Pinedo, B.D. Metzger, MNRAS 463, 2323 (2016). https://doi.org/10.1093/mnras/stw2156
- M.R. Wu, J. Barnes, G. Martínez-Pinedo, B.D. Metzger, Phys. Rev. Lett. 122, 062701 (2019). https://doi.org/10.1103/ PhysRevLett.122.062701
- S. Wanajo, Y. Sekiguchi, N. Nishimura, K. Kiuchi, K. Kyutoku, M. Shibata, Astrophys. J. 789, L39 (2014). https://doi.org/10.1088/2041-8205/789/2/L39
- O. Just, A. Bauswein, R.A. Pulpillo, S. Goriely, H.T. Janka, MNRAS 448, 541 (2015). https://doi.org/10.1093/mnras/stv009
- A. Bauswein, O. Just, H.T. Janka, N. Stergioulas, Astrophys.
   J. Lett. 850, L34 (2017). https://doi.org/10.3847/2041-8213/aa9994
- J.M. Miller, B.R. Ryan, J.C. Dolence, A. Burrows, C.J. Fontes, C.L. Fryer, O. Korobkin, J. Lippuner, M.R. Mumpower, R.T. Wollaeger, Phys. Rev. D 100(2), 023008 (2019). https://doi.org/10.1103/PhysRevD.100.023008
- J. Barnes, Y.L. Zhu, K.A. Lund, T.M. Sprouse, N. Vassh, G.C. McLaughlin, M.R. Mumpower, R. Surman, Astrophys. J. 918(2), 44 (2021). https://doi.org/10.3847/1538-4357/ac0aec
- K.A. Lund, J. Engel, G.C. McLaughlin, M.R. Mumpower, E.M. Ney, R. Surman, arXiv e-prints arXiv:2208.06373 (2022)
- A.P. Ji, M.R. Drout, T.T. Hansen, Astrophys. J. 882, 40 (2019). https://doi.org/10.3847/1538-4357/ab3291
- B.E.J. Pagel, Nucleosynthesis and Chemical Evolution of Galaxies, 2nd edn. (Cambridge University Press, Cambridge, 2009). https://doi.org/10.1017/CBO9780511812170
- F. Matteucci, Chem. Evolut. Galax. (2012). https://doi.org/10. 1007/978-3-642-22491-1
- K. Nomoto, C. Kobayashi, N. Tominaga, Ann. Rev. Astron. Astrophys. 51, 457 (2013). https://doi.org/10.1146/ annurev-astro-082812-140956

 N. Prantzos, C. Abia, M. Limongi, A. Chieffi, S. Cristallo, MNRAS 476(3), 3432 (2018). https://doi.org/10.1093/mnras/ sty316

- N. Prantzos, C. Abia, S. Cristallo, M. Limongi, A. Chieffi, MNRAS 491(2), 1832 (2020). https://doi.org/10.1093/mnras/ stz3154
- C. Kobayashi, A.I. Karakas, M. Lugaro, Astrophys. J. 900(2), 179 (2020). https://doi.org/10.3847/1538-4357/abae65
- F. Matteucci, Ann. Rev. Astron. Astrophys. 29(1), 5 (2021). https://doi.org/10.1007/s00159-021-00133-8
- G. Cescutti, F. Matteucci, Universe 8(3), 173 (2022). https://doi. org/10.3390/universe8030173
- C. Sneden, J.J. Cowan, R. Gallino, Ann. Rev. Astron. Astrophys.
   46, 241 (2008). https://doi.org/10.1146/annurev.astro.46.060407.
   145207
- T. Fischer, M.R. Wu, B. Wehmeyer, N.U.F. Bastian, G. Martínez-Pinedo, F.K. Thielemann, Astrophys. J. 894(1), 9 (2020). https:// doi.org/10.3847/1538-4357/ab86b0
- T. Suda, Y. Katsuta, S. Yamada, T. Suwa, C. Ishizuka, Y. Komiya, K. Sorai, M. Aikawa, M.Y. Fujimoto, Publ. Astron. Soc. Jpn. 60, 1159 (2008). https://doi.org/10.1093/pasj/60.5.1159
- 104. H. Schatz, R. Toenjes, B. Pfeiffer, T.C. Beers, J.J. Cowan, V. Hill, K.L. Kratz, Astrophys. J. 579, 626 (2002). https://doi.org/10.1086/342939
- I.U. Roederer, K.L. Kratz, A. Frebel, N. Christlieb, B. Pfeiffer, J.J. Cowan, C. Sneden, Astrophys. J. 698, 1963 (2009). https:// doi.org/10.1088/0004-637X/698/2/1963
- I.U. Roederer, C. Sneden, J.E. Lawler, J.J. Cowan, Astrophys. J. 714, L123 (2010). https://doi.org/10.1088/2041-8205/714/1/ L123
- L. Mashonkina, N. Christlieb, K. Eriksson, Astron. Astrophys.
   569, A43 (2014). https://doi.org/10.1051/0004-6361/201424017
- I.U. Roederer, Astrophys. J. 835, 23 (2017). https://doi.org/10. 3847/1538-4357/835/1/23
- E.M. Holmbeck, T.C. Beers, I.U. Roederer, V.M. Placco, T.T. Hansen, C.M. Sakari, C. Sneden, C. Liu, Y.S. Lee, J.J. Cowan, A. Frebel, Astrophys. J. 859, L24 (2018). https://doi.org/10.3847/2041-8213/aac722
- T.T. Hansen, E.M. Holmbeck, T.C. Beers, V.M. Placco, I.U. Roederer, A. Frebel, C.M. Sakari, J.D. Simon, I.B. Thompson, Astrophys. J. 858, 92 (2018). https://doi.org/10.3847/1538-4357/ aabacc
- C.M. Sakari et al., Astrophys. J. 868, 110 (2018). https://doi.org/ 10.3847/1538-4357/aae9df
- E.M. Holmbeck et al., Astrophys. J. Suppl. 249(2), 30 (2020). https://doi.org/10.3847/1538-4365/ab9c19
- R. Ezzeddine et al., Astrophys. J. 898(2), 150 (2020). https://doi. org/10.3847/1538-4357/ab9d1a
- E.M. Holmbeck, A. Frebel, G.C. McLaughlin, M.R. Mumpower, T.M. Sprouse, R. Surman, Astrophys. J. 881, 5 (2019). https://doi. org/10.3847/1538-4357/ab2a01
- F. Matteucci, D. Romano, A. Arcones, O. Korobkin, S. Rosswog, MNRAS 438, 2177 (2014). https://doi.org/10.1093/mnras/ stt2350
- B. Wehmeyer, M. Pignatari, F.K. Thielemann, MNRAS 452, 1970 (2015). https://doi.org/10.1093/mnras/stv1352
- G. Cescutti, D. Romano, F. Matteucci, C. Chiappini, R. Hirschi, Astron. Astrophys. 577, A139 (2015). https://doi.org/10.1051/ 0004-6361/201525698
- F. van de Voort, R. Pakmor, R.J.J. Grand, V. Springel, F.A. Gómez,
   F. Marinacci, MNRAS 494(4), 4867 (2020). https://doi.org/10. 1093/mnras/staa754
- 119. F. van de Voort, R. Pakmor, R. Bieri, R.J.J. Grand, MNRAS 512(4), 5258 (2022). https://doi.org/10.1093/mnras/stac710



12 Page 14 of 14 Eur. Phys. J. A (2023) 59:12

- J.J. Cowan, C. Sneden, T.C. Beers, J.E. Lawler, J. Simmerer, J.W. Truran, F. Primas, J. Collier, S. Burles, Astrophys. J. 627, 238 (2005). https://doi.org/10.1086/429952
- 121. A. Abohalima, A. Frebel, Astrophys. J. Suppl. **238**(2), 36 (2018). https://doi.org/10.3847/1538-4365/aadfe9
- S. Wanajo, Y. Hirai, N. Prantzos, MNRAS 505(4), 5862 (2021). https://doi.org/10.1093/mnras/stab1655
- Y. Hirai, T.C. Beers, M. Chiba, W. Aoki, D. Shank, T.R. Saitoh, T. Okamoto, J. Makino, MNRAS 517(4), 4856 (2022). https://doi.org/10.1093/mnras/stac2489
- 124. C. Kobayashi, I. Mandel, K. Belczynski, S. Goriely, T.H. Janka, O. Just, A.J. Ruiter, D. Van Beveren, M.U. Kruckow, M.M. Briel, J.J. Eldridge, E. Stanway, arXiv e-prints arXiv:2211.04964 (2022)

